An Approach towards the Measurement of Nanometer Range Distances Based on Cu^{2+} Ions and ESR

Zhongyu Yang, Drew Kise, and Sunil Saxena*

Department of Chemistry, University of Pittsburgh, Pittsburgh, Pennsylvania 15260

Received: December 8, 2009; Revised Manuscript Received: March 29, 2010

We present the measurement of $Cu^{2+}-Cu^{2+}$ and $Cu^{2+}-$nitroxide distance distributions using double electron−electron resonance (DEER) on a proline-based peptide and an alanine-based peptide. The proline-based peptide contains two well-characterized Cu^{2+} binding segments, PHGGGW, separated by seven proline residues. The alanine-based peptide contains a PHGGGW segment at one end of the peptide and a nitroxide spin label attached to a cysteine residue close to the other end of the peptide. DEER experiments were performed at several external magnetic fields and resonance offsets to probe the orientational effects on the Cu^{2+}-based DEER signal. Subtle but detectable orientational effects were observed from the DEER spectra of both peptides. A general theoretical model was developed to analyze the experimental data sets. We show that the Tikhonov regularization-based method is not applicable to extract precise Cu^{2+}-based distance distributions. Instead, a full data analysis is required to obtain the distance distributions and relative orientations between spin centers. A 30 Å mean $Cu^{2+}-Cu^{2+}$ distance and a 27 Å mean $Cu^{2+}-$nitroxide distance were determined in the two peptides. These distances are consistent with structural models and with earlier measurements. Constraints on the relative orientation between paramagnetic centers in these two model peptides were determined by examination of the orientational effects. The data analysis procedure is system independent, and therefore is applicable to more complicated biological systems.

Introduction

Double electron electron resonance (DEER)[1–4] has become a powerful approach to measure interspin distance distributions in the range 2−8 nm. The distribution of distances provides valuable structural information in order to probe the structure and dynamics of soluble proteins,[5–18] DNA and RNA,[19–24] and oligomers.[25–32] The DEER technique is attractive because it can provide distance constraints even in membrane proteins[33–45] and large biomolecular complexes.[10,46,47] The paramagnetic centers employed are mostly nitroxide spin labels, which are covalently attached to a cysteine residue in a biomolecule by site-directed spin labeling.[48–50] Nitroxide−nitroxide distance distributions can be precisely determined by utilizing an inversion technique based on Tikhonov regularization.[51,52] Recently, paramagnetic metal ions have also been employed as the spin centers.[5,6,52–58] The data analysis procedures for metal ion centers, on the other hand, are still under development.

In principle, the selective microwave pulses applied in the DEER experiment excite only a small portion of the ESR spectrum. This partial selectivity of the ESR spectrum can impart the so-called "orientational selectivity" on the DEER signal. For the case of nitroxide spin labels, the distance distribution can often be resolved by using an inversion technique based on Tikohonov regularization.[51,52] The Tikhonov regularization method extracts the distance distribution by solving a Fredholm equation containing a kernel that is readily available from theory. The kernel for nitroxide spin labels is simplified, since effects due to relative orientations of the two spin centers are typically randomized, due to the large inherent flexibility of the spin labels.[51,52] However, in some specific cases, the nitroxide orientational selectivity can be observed.[2] For instance, Prisner and co-workers observed a frequency offset dependence on the nitroxide-based DEER signal in the potassium ion channel, KcsA, even at the X-band.[59] In this protein, the nitroxide spin labels were orientationally restricted due to the tertiary interaction. Such strong restriction of the nitroxide spin labels in the membrane protein made the Tikhonov regularization method problematic in extracting nitroxide−nitroxide distances. Instead, a full analysis of these frequency offset dependent DEER data was required. By using a molecular model, Prisner and co-workers were able to resolve not only the nitroxide−nitroxide distances but also the orientations of nitroxide spin labels at the X-band.[59] Orientational effects on the nitroxide-based DEER signal also become more significant at higher resonance frequencies, where a full data analysis procedure is also required to obtain information on distances as well as the relative orientation of the spin labels.[60,61]

For the case of paramagnetic metal ions such as Cu^{2+}, the importance of accounting for orientational effects has been noticed by us as well as other research groups.[5,53,54,56,57] In most of these works, DEER data were collected at several magnetic fields and/or frequency offsets, and distances were measured by an analysis based on an appropriate theoretical model. In an elegant contribution from Prisner and co-workers, a procedure was developed for a model compound where the Cu^{2+} and the spin label were separated by a fairly rigid linker.[56] In a more recent work, Lovett et al. developed another procedure to extract the distance as well as the relative orientation between two Cu^{2+} in a dicopper complex.[57] In both cases, the structural information such as the location, the electron spin density delocalization, the orientation of each spin center, and the flexibility of the linker between spin centers could be estimated by X-ray diffraction measurements and/or DFT calculations. The avail-

* Author to whom correspondence should be addressed. Phone: 412 624 8680. Fax: 412 624 8611. E-mail: sksaxena@pitt.edu.

10.1021/jp911637s
Published on Web 04/16/2010

ability of such structural information simplified the data analysis procedures. These works were important in establishing the role of the spin density delocalization on Cu^{2+}-based distances. On the basis of the understanding obtained by these works, we sought to develop a more general analysis procedure that can be applicable to an unknown sample or a more complicated biomolecule, where DFT calculations are not accessible.

The key step to making our procedure general is to use a molecular model, wherein the relative orientation of the principal axes system of the two spin centers was described by three Euler angles; these angles were allowed to have a distribution. No structural information regarding the linker between the spin centers, or the precise distance, is required to analyze the DEER signal, which therefore ensures that this model is system independent. The model was tested on two synthetic peptides, one with Cu^{2+} bound to both ends of the peptide and the other with one Cu^{2+} bound to one end and one nitroxide attached to the other end of the peptide. Experimental DEER data showed only very subtle frequency offset dependence for the alanine-based peptide. Detectable magnetic field dependence was observed for the proline-based peptide data sets. These data sets were analyzed using our model, wherein both spin−spin distance distributions and relative orientations between spin centers were determined for the two peptides. These parameters were consistent with results of molecular modeling.[62–65] The success of the present analysis procedure indicates that our model can be applied to more complicated biological systems.

Theory and Experimental Methods

Theory. DEER data can be orientationally selective due to the mechanism by which DEER measures the dipolar interaction, ω_{dd}:

$$\omega_{dd} = -\frac{\mu_0 \mu_B^2}{4\pi\hbar}\frac{g_1 g_2}{r^3}(3\cos\theta^2 - 1) \qquad (1)$$

In eq 1, μ_B is the Bohr magneton, g_1 and g_2 are the g-values of the coupled electron spins, $\hbar$ is the Planck constant divided by 2π, r is the spin−spin distance, θ is the angle between the spin−spin vector $\mathbf{r}$ and the external magnetic field, and μ_0 is the vacuum permeability. The dipolar frequency as shown in eq 1 depends on r and the θ angles that are excited. For the case of nitroxide spin labels, the relative orientations of the two spin centers are randomized due to the inherent flexibility of the spin label. The microwave pulses, used in DEER experiments, therefore, can uniformly excite most of the θ values. Assuming most of the θ are excited by the pulses, the Tikhonov method with a simplified kernel can be used to measure distance distributions.[52] For the cases of higher resonance frequencies[60,61] (>90 GHz), restricted label motions,[59] or Cu^{2+}-based DEER experiments, this approach to extract interspin distances can be questionable.

For the case of Cu^{2+} at X-band, the large g and hyperfine anisotropies broaden the Cu^{2+} ESR spectrum to ~2 GHz, compared with a 200 MHz nitroxide ESR spectrum (cf. Figure 1). The coverage of microwave pulses used in the DEER experiments is typically ~20−50 MHz, and thus, only a small portion of the Cu^{2+} ESR spectrum is excited (cf. Figure 1b and below). The high-field part of the X-band Cu^{2+} spectrum is highly disordered because of the interplay of g and A anisotropies, in combination with $I = 3/2$. Therefore, in the experimental setup, if both the observation and pumping pulses excite the high-field part of the spectrum, the range of angles θ contributing

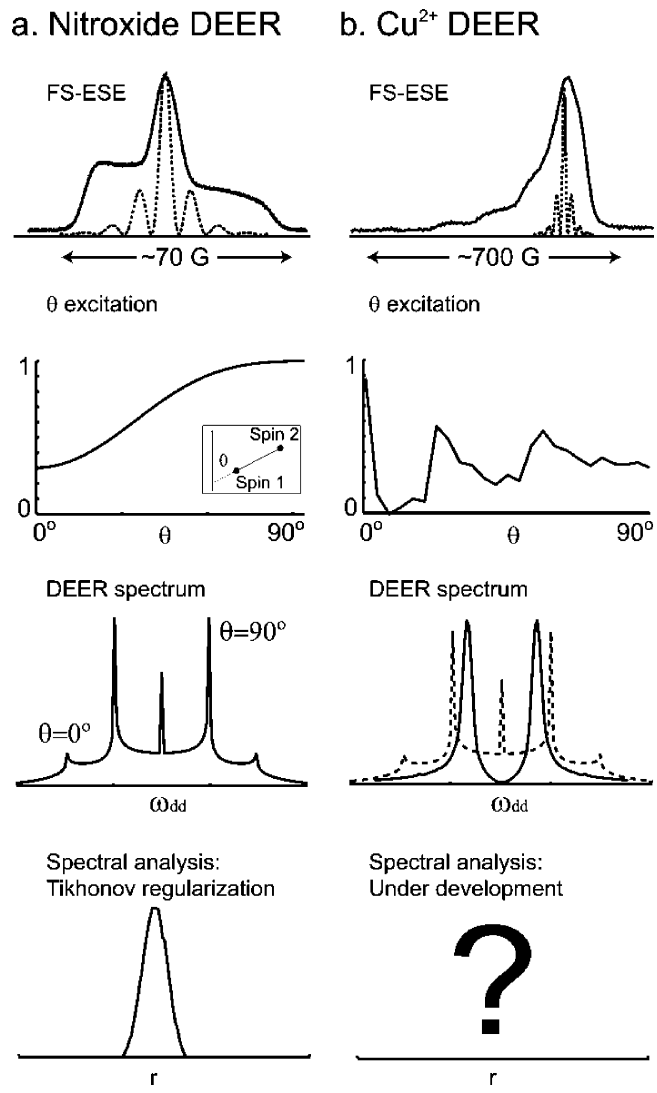

Figure 1. Field-swept electron spin echo (FS-ESE) spectrum, simulated θ excitation profile, and simulated DEER spectrum for a nitroxide sample (a) and a Cu^{2+} sample (b), respectively. The coverage of the microwave pulse used in DEER is shown by the dashed line in both figures. For the case of nitroxide, most θ angles are excited, resulting in the familiar Pake pattern shown in part a. For the case of Cu^{2+}, however, the θ excitation profile is not uniform and therefore the measured DEER spectrum differs from the Pake pattern (b).

to DEER effect can be broad, which can dilute the orientational selectivity effects. However, they may still affect the resultant DEER spectrum. Consequently, the spectrum may differ from a Pake pattern (cf. Figure 1b). The excited θ angles are in general unknown and dependent on the relative orientation of the two spin centers. The distance between Cu^{2+} centers cannot be extracted using the Tikhonov method with a simplified kernel (cf. Figure 1b) but becomes dependent on the θ excitation profile. The θ excitation profile can be quantitatively analyzed using known procedures (cf. the Supporting Information).

To account for the orientational effects, the total DEER signal can be expressed as[66]

$$V(T) = \iint P(r)\xi(\theta)\langle 1 - \cos[\omega_D(1 - 3\cos^2\theta) + J]T\rangle \, d\theta \, dr \qquad (2)$$

where

$$\xi(\theta) = \frac{1}{2}\sum_{m_{I_1},m_{I_2}} \langle k_{xa}{}^3 k_{xb}{}^2 \sin\varphi_{1a}(1-\cos\varphi_{2a})(1-\cos\varphi_{3b}) + k_{xb}{}^3 k_{xa}{}^2 \sin\varphi_{1b}(1-\cos\varphi_{2b})(1-\cos\varphi_{3a})\rangle_{\Phi,\delta\omega_1,\delta\omega_2}$$

is the full expression of the geometrical factor; $P(r)$ is the probability of distances. m_{I_i} ($i = 1, 2$) is the nuclear quantum number of the ith spin center; φ_{ia} ($i = 1, 2, 3$) is the flip angle of the first spin caused by the ith pulse in the three-pulse DEER pulse sequence; φ_{ib} ($i = 1, 2, 3$) is the flip angle of the second spin caused by the ith pulse in the three-pulse DEER pulse sequence; $\delta\omega_i$ ($i = 1, 2$) denotes the inhomogeneous broadening of the ESR spectrum excited by the observer ($i = 1$) or the pump pulses ($i = 1$). k_{xa} is defined as the ratio of the actual resonance frequency of the spins excited by the observer pulses versus the observer frequency; k_{xb} is defined as the ratio of the actual resonance frequency of the spins excited by the pump pulse versus the pump frequency. More details of the definition of variables in eq 2 are shown by Maryasov et al.[66] To extract precise Cu^{2+}-based spin−spin distances and relative orientations between spin centers, both the interspin distance and the geometrical factor need to be considered in the data analysis procedure.

The Molecular Model. The model is illustrated using the proline-based peptide which contains two copper centers. The g-tensor of the Cu^{2+} close to the N-terminal of the peptide (also referred to as the first Cu^{2+} in this work) was chosen to be the reference frame (cf. Figure 2).[67,68] The Cu^{2+} center in the C-terminal of the peptide can also be used as the reference frame. This will not affect the molecular model, the fitting procedure, and the relative orientation between the two Cu^{2+} centers. The relative position between the two copper atoms was described by a vector, **R**, and an angle, χ (cf. Figure 2). The relative orientation of the two Cu^{2+} g-tensors was described by two Euler angles, γ and η. Only three angles are required to describe the geometry of the two spin centers because of the axial symmetry of the two Cu^{2+} principal axes system. The geometrical factor as shown in eq 2 depends only on the relative orientation between the principal axes system of the two spin centers (cf. the Supporting Information). Therefore, the definition of the reference frame generates no ambiguity. To account for the flexibility of the peptide, the position of each copper atom in this model was assumed to be localized randomly within a spherical region. The radius of the sphere was denoted as ΔR. The angles χ, γ, and η were also assumed to be flexible within certain ranges. In our approach, we generated an ensemble containing 2000 different locations of the spin center using a Monte Carlo procedure (see the Supporting Information). The DEER signal was calculated for each location, and the 2000 signals were summed up to generate the total DEER signal. This signal depended on parameters such as the distance distribution as well as on the relative orientation. The DEER signal was compared to experiment, and the parameters were varied until a good fit was reached. Details of signal calculations are provided in the Supporting Information.

Strategy to Optimize the Variables in the Model. Variables in the molecular model to be optimized are R, ΔR, χ, γ, η, σ_χ, σ_γ, and σ_η. For an unknown model peptide, there is no information regarding the exact value of each variable. However, estimation of the range of each variable can still be made on the basis of properties of the sample molecules and spin centers. For instance, for both peptide sequences, the length between spin centers can be estimated to be in the range 20−40 Å. The relative orientations of the two spin centers were expected to contain similar flexibility in the direction of the x, y, or z axis of the reference frame. Therefore, to a good approximation, we set $\sigma_\chi \approx \sigma_\gamma \approx \sigma_\eta$ at a value of σ. We then randomly chose values for the three angles and the standard deviation as the initial inputs and calculated the correlation of R and ΔR, by generating a contour plot of average χ^2 values in functions of R and ΔR using eq S16 from the Supporting Information. The lowest χ^2 value represented the best R and ΔR when the Euler angles and σ were applied at initial inputs. We then fixed R and ΔR at these optimized values, randomly chose a value for σ, and varied χ, γ, and η by increments of 30° ranging from 0 to 90° to calculate the average χ^2 values to find the best Euler angles. Third, we kept R, ΔR, χ, γ, and η at the preoptimized values and varied the σ value by increments of 3°, to determine the optimized standard deviation for each Euler angle. Once the Euler angles and the standard deviation were optimized, the correlation of R and ΔR was calculated again to ensure that the optimized R and ΔR values remained. If a new set of R and ΔR values was obtained, the same steps to optimize the Euler angles and standard deviations were performed again until self-consistent results were obtained.

The robustness and specificity of the optimized variables were further tested by using different initial inputs. For example, we used a different set of Euler angles to investigate the best R and ΔR values, and then optimized the angles and the standard deviation. We even tried to randomly choose the values for R and ΔR as the initial inputs and optimized the angles first, and then use the optimized angles to optimize the R and ΔR. The optimized variables were found to be unchanged for both peptides.

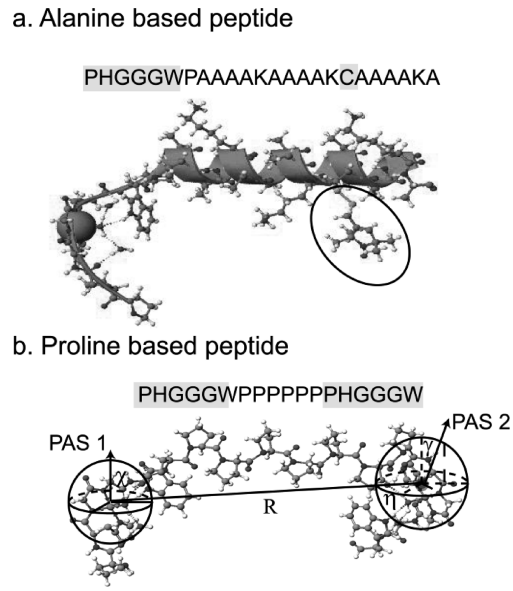

Figure 2. (a) The molecular structure of the alanine-based peptide, as adapted from Jun et al., *Biochemistry* **2006**, *45*, 11666−11673. The Cu^{2+} center is highlighted using the space-filling method. The nitroxide spin label is indicated by the circle. (b) The definition of the relative orientation of the two spin centers overlapped on a raw molecular structure of the proline-based peptide. This structure was built based on previous proline-based peptide work from Becker et al., *Chem. Phys. Lett.* **2005**, *414*, 248. The peptide sequences for both peptides are also shown.

Sample Preparations. ***Alanine-Based Peptide Sample.*** The sequence of the alanine-based peptide is PPHGGGWPAAAA-KAAAAKCAAAAKA (cf. Figure 2a; P, proline; H, histidine; G, glycine; W, tryptophan; A, alanine; K, lysine; C, cysteine).

This peptide was synthesized at the Molecular Medicine Institute, University of Pittsburgh. The lysine residues in this peptide increase the solubility of the peptide in aqueous solutions. The PHGGGW on one end of the peptide serves as a copper binding sequence.[67,69,70] The purpose of the cysteine residue close to the other end of the peptide was to covalently attach the (1-oxy-2,2,5,5-tetramethylpyrroline-3-methyl) methanethiosulfonate (MTSSL) spin label, using site-directed spin labeling (SDSL). The spin labeled alanine-based peptide was mixed with 25 mM *N*-ethylmorpholine (NEM) buffer and 25% glycerol, and the pH value of the mixture was adjusted to be 7.4−7.6. The concentration of the peptide sample was 1.2 mM. Isotopically enriched $^{63}CuCl_2$ was dissolved in the same buffer as for the peptide solution with the same pH value to make the Cu^{2+} stock solution. Cu^{2+} was then mixed with the peptide solution with a 1:1 Cu^{2+} to peptide ratio. On the basis of the binding affinity of Cu^{2+} to the PHGGGW segment, more than 88% of the Cu^{2+} was bound to the peptide.[65]

Proline-Based Peptide Sample. The peptide sequence of the proline-based peptide is PPHGGGWPPPPPPPHGGGW. This peptide was also synthesized at the Molecular Medicine Institute, University of Pittsburgh. The proline-based peptide was mixed with 25 mM *N*-ethylmorpholine (NEM) buffer and 25% glycerol, and the pH value of the mixture was adjusted to be 7.4−7.6. The concentration of the peptide sample was 1.6 mM. Isotopically enriched $^{63}CuCl_2$ was dissolved in the same buffer with the same pH value to make the Cu^{2+} stock solution. Cu^{2+} was then mixed with the peptide solution with a 6:1 Cu^{2+} to peptide ratio to ensure that both PHGGGW sites were occupied by Cu^{2+}.

ESR Experiments. All of the pulsed ESR experiments were performed on a Bruker Elexsys 580 spectrometer at 20 K. A MD5 resonator was used in all of the experiments. The effective sample volumes for both samples were ∼120 μL.

The three pulse ESEEM signals were collected by recording the stimulated electron spin echo intensity as a function of T using the sequence $(\pi/2)$-τ-$(\pi/2)$-T-$(\pi/2)$-τ-(stimulated echo) on both peptides. The duration of the $(\pi/2)$ pulses was 16 ns. The interpulse delay τ was fixed at 200 ns. The time interval T was incremented from 400 ns with a step size of 16 ns, for a total of 1024 points. A four-step phase cycle was employed to eliminate unwanted signals.[4]

For the DEER experiments, a $(\pi/2)_{v_1}$-τ_1-$(\pi)_{v_1}$-T-$(\pi)_{v_2}$-τ_2-$(\pi)_{v_1}$-τ_1 echo was employed. The pulse duration of the $(\pi/2)_{v_1}$, $(\pi)_{v_1}$, and $(\pi)_{v_2}$ pulses was adjusted to be 24, 48, and 36 ns, respectively. However, for the DEER data on the proline-based peptide at 3060 G, the pump pulse legnth was set to be 16 ns using a MPFU channel. For the alanine-based peptide, the interval T was incremented from 136 ns with a stepsize of 12 ns, for a total of 128 points. Proton modulation was averaged by adding traces at four different τ_1 values, starting at 200 ns and incrementing by 18 ns.[2] Interval τ_2 was adjusted to make $(\tau_1 + \tau_2) = 1700$ ns. A two-step phase cycling $(+x, -x)$ was carried out on the first $(\pi/2)$ pulse. For the proline-based peptide at higher magnetic field (>3230 G), the interval T was incremented from 144 ns with a stepsize of 16 ns, for a total of 128 points. At 3060 G, the stepsize applied was 10 ns, with the same number of points. A similar procedure was applied to reduce the effect from proton ESEEM as in the alanine-based peptide sample.

To measure the distance between Cu^{2+} and the spin label in the alanine-based peptide, the pump and observer pulses were placed at the nitroxide and Cu^{2+} ESR spectrum, respectively. Four different frequency offsets, 260, 364, 448, and 560 MHz, were maintained to probe the orientational effects on the DEER signal. The relative position of the pump and observer frequencies is shown in the Figure 3a inset. The signal collection time varied from 4 to 16 h, depending on the frequency offset.

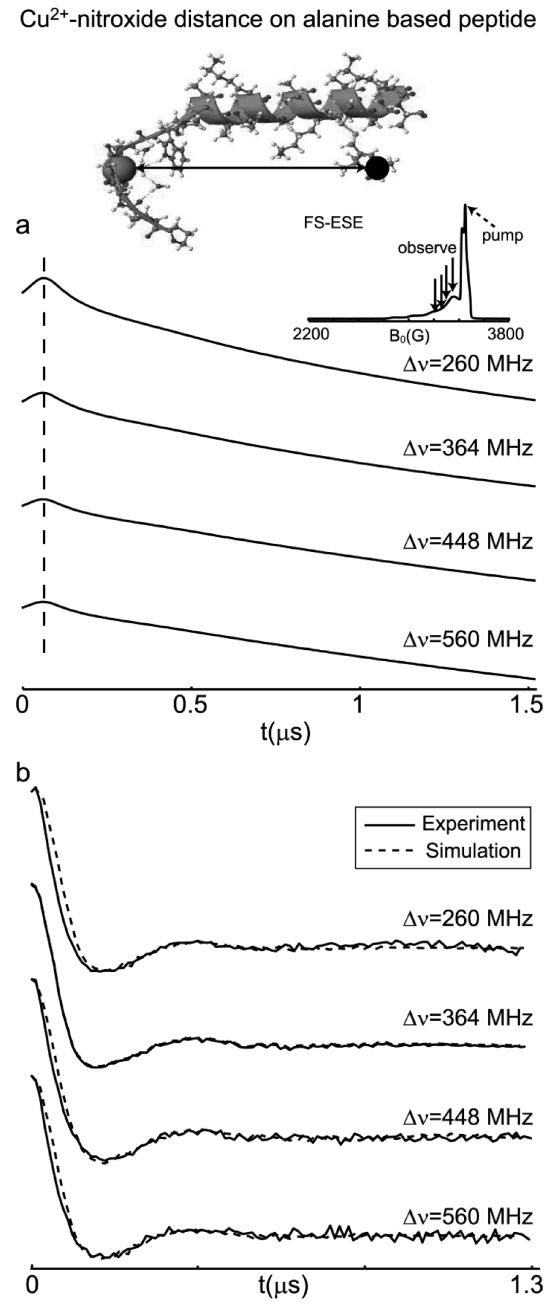

Figure 3. (a) Experimental DEER time domain traces for the alanine-based peptide at four different frequency offsets between 260 and 560 MHz. The vertical dashed line indicates the zero time of each trace. (Inset) The FS-ESE spectrum with the pump and observer frequencies used in DEER shown by arrows. (b) DEER signal after the removal of the intermolecular decay by division of an exponential decay. A clear modulation can be observed at ∼200 ns, for all of the experimental data sets. These baseline corrected DEER data were fit by using the theoretical model developed in this work. Simulations are shown by dashed lines.

To measure the Cu^{2+}−Cu^{2+} distance in the proline-based peptide, both the pump and observer frequencies were applied to the Cu^{2+} ESR spectrum. DEER signals were collected at five different magnetic fields, 3320, 3290, 3260, 3230, and 3060 G. The signal collection time was 8−72 h depending on the different magnetic fields. DEER signals were also collected for two different frequency offsets, 200 and 300 MHz.

Results

DEER on the Alanine-Based Peptide. The alanine-based peptide contains a Cu^{2+} center and a nitroxide spin label. Prior to DEER experiments, the Cu^{2+} binding environment in the alanine-based peptide was confirmed by using three-pulse electron spin echo envelop modulation (ESEEM) spectroscopy. The resultant ESEEM spectrum showed characteristic peaks due to electron nuclear dipolar interactions between the unpaired Cu^{2+} electron and ^{14}N nuclear spins from both a histidine residue and a noncoordinated glycine residue (data not shown).[69] These peaks are signatures of Cu^{2+} binding to the prion protein copper binding segment, PHGGGW.[67]

The experimental DEER traces for the alanine-based peptide are shown in Figure 3a. The pump pulse was applied at the maximum position of the nitroxide ESR spectrum, as shown by the dashed arrow in the inset to Figure 3a. The observer pulses were applied at four different resonance offsets, as indicated by the solid arrows in the inset to Figure 3a, that range from 260 to 560 MHz. The zero time of each data set was precisely determined and illustrated by the dashed line in Figure 3a. A slight but noticeable modulation occurring at ~200 ns can be observed in all of the data sets. The modulation depth varied in the range 5−10% depending on different frequency offsets. This range is comparable to the theoretical values which gave a range of 7−12%[1] (the slight difference is possibly caused by the inhomogeneous excitation of the mw B_1-field[29]). Depending on the observer frequency, the DEER data show different decaying slopes due to the intermolecular interaction. The background signal for each data set was fit by an exponential function and removed from the original data. The baseline corrected DEER traces are shown in Figure 3b. The differences between these DEER traces are difficult to visualize. However, a Fourier transformation of each data set shows subtle differences between different data sets in the frequency domain, indicating a weak orientational selectivity (data not shown).

The alanine-based peptide was earlier used by Jun et al. to measure the average distance between Cu^{2+} and the nitroxide spin label based on T_1 measurements and molecular dynamics simulations.[65] On the basis of their MD model, the initial Euler angles were selected to be $\chi = 90°$, $\gamma = 0°$, and $\eta = 60°$.[65] A combination of the peptide backbone flexibility and nitroxide side chain flexibility creates large flexibilities in the three Euler angles. As initial inputs, we set the standard deviation at 20°. This value together with the initial Euler angle inputs were optimized later in this section. The radius of the sphere in which the nitroxide spin is located, namely, $\Delta R'$, is not necessary to be the same as the Cu^{2+} sphere. Initially, we set $\Delta R' = \Delta R$ and in later simulations investigated the best radius of the nitroxide sphere. Using these initial inputs, the correlation of R and ΔR was calculated and shown in Figure 4a. The best fit occurred at $R = 27$ Å and $\Delta R = 3$ Å. We then fixed R and ΔR at the optimized values and optimized χ, γ, η, and σ, as explained in the method section. The best fit occurs at $(\chi, \gamma, \eta) = (90°, 30°, 30°)$ and $\sigma = 9-12°$. Lastly, we varied $\Delta R'$ and ΔR in the range 1−5 Å to investigate the best fit and determined that the best fit occurred at $\Delta R' = \Delta R = 3$ Å. Most likely, the flexibility of the peptide backbone is the major contributor to the flexibility in the locations of the spin centers. Using the optimized parameter set, the relative orientation between Cu^{2+} and nitroxide g-tensors can be illustrated by the black dots shown in Figure 4b.

The specificity of the optimized Euler angles—$\chi = 90°$, $\gamma = 30°$, and $\eta = 30°$—and $\sigma = 9-12°$ was further examined by investigating the change of the average χ^2 values upon changing

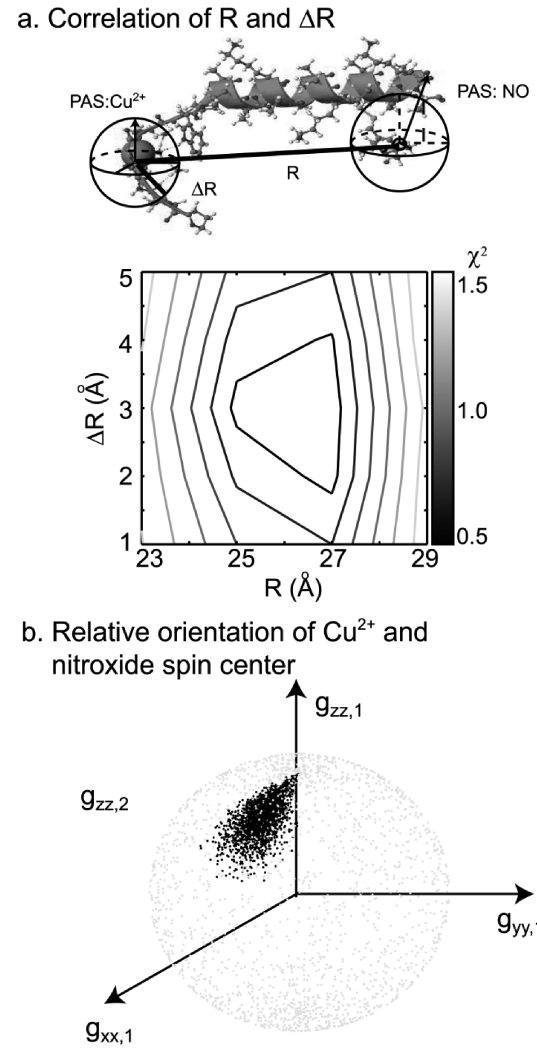

Figure 4. (a) Correlation between R and ΔR, using initial inputs of $\chi = 90°$, $\gamma = 0°$, and $\eta = 60°$. The lowest χ^2 value occurs at $R = 27$ Å, $\Delta R = 3$ Å, $\chi = 90°$, $\gamma = 30°$, and $\eta = 30°$. (b) Orientations of the nitroxide g_{zz} axis with respect to the Cu^{2+} g-tensor shown by black dots.

parameters. Representative fittings are shown in Figures 5−7. Our results showed that the χ angle played the most important role. Figure 5 shows the fitting of the first 600 ns of the time domain traces for three experimental data sets, by scanning χ values from 0 to 90°, using $\gamma = 30°$ and $\eta = 30°$. The χ^2 values are listed near each fitting curve. Both visual inspection and χ^2 values show that the best χ value occurs at 90°, with corresponding χ^2 values of 0.0802, 0.062, and 0.104 for the three experimental data sets. When the χ value deviated from 90°, the χ^2 value increased more than 3-fold. Similarly, in Figures 6 and 7, we show the effects of γ and η on the fitting of the experimental data. The changes in χ^2 values by changing the γ and η angles were not as significant as changing the χ values (cf. listed χ^2 values in Figures 6 and 7). However, different γ and η angles still provided different fits to the experimental data. For instance, as shown in Figure 6, $\gamma = 0°$ provides good fits to experimental data at 260 and 364 MHz frequency offsets with corresponding χ^2 values of 0.0838 and 0.0485, respectively. At 448 MHz resonance offset, however, the χ^2 increased to 0.121. Similarly, as shown in Figure 7, using $\eta = 0°$, the fit to the experimental data with 448 MHz resonance offset, was actually better than using $\eta = 30°$, as shown by the χ^2 values. However, the fits to the other two experimental data sets were

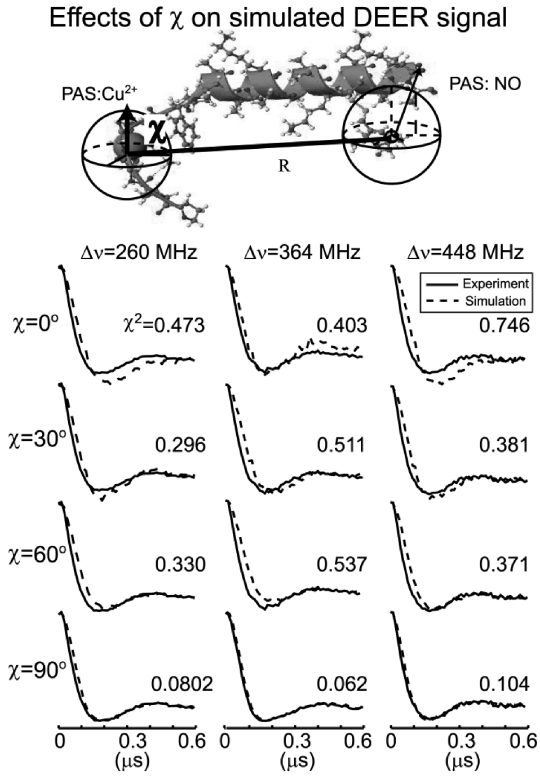

Figure 5. Investigation of the effect of the χ angle on the DEER simulation. Representative fitting of three experimental data using χ values varying from 0 to 90° are shown. The χ^2 values for each fitting are also listed. For all experimental data, the best χ value is 90°.

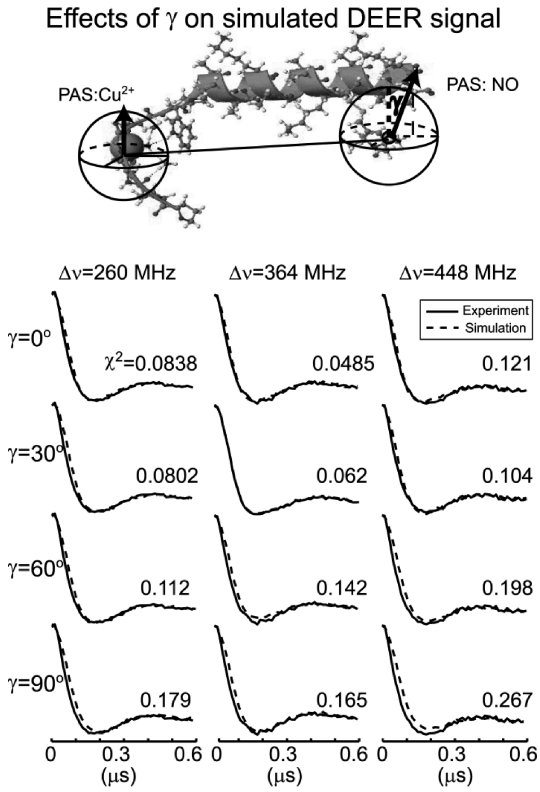

Figure 6. Investigation of the effect of the γ angle on the DEER simulation. Representative fitting of three experimental data using γ values varying from 0 to 90° are shown. The χ^2 values for each fitting are also listed. For all experimental data, the best γ value is 30°.

not acceptable. The optimized σ was also investigated in a similar manner. We observed that σ values below 9° led to a

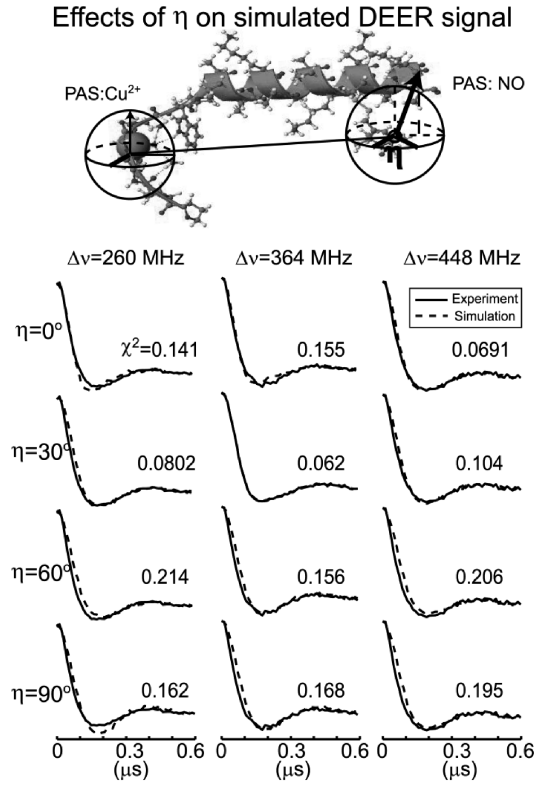

Figure 7. Investigation of the effect of the η angle on the DEER simulation. Representative fitting of three experimental data using η values varying from 0 to 90° are shown. The χ^2 values for each fitting are also listed. For all experimental data, the best η value is 30°.

simulated signal with a higher modulation amplitude compared with the experimental data, resulting in a "bad" fit. Conversely, σ values above 12° led to a lower modulation amplitude compared with the experimental data, also resulting in a "bad" fit. The weak orientational selectivity did not change the distance distribution function between spin centers but could be used to isolate the best orientational parameters.

Five different initial inputs were tested in the fitting procedure. In all cases, we obtained the same optimized Euler angles of $\chi = 90°$, $\gamma = 30°$, and $\eta = 30°$ and a standard deviation of $\sigma = 9-12°$. The distance distribution function was also unchanged. Using the optimized parameters, the Cu^{2+}−nitroxide distance distribution was calculated by a statistical histogram plot of the spin−spin distances for 2000 conformations and shown by the solid line in Figure 8a. The mean distance and the standard deviation were calculated to be 27 and 2.4 Å, respectively. The mean distance is consistent with relaxation results (see below).[65] The standard deviation is also in agreement with literature estimates of polyalanine peptides.[62] The large values of σ are reasonable given that a small bending of the polypeptide chain can lead to a large change in the relative orientation. Using the determined Euler angles and standard deviations of Euler angles, the model of the alanine-based peptide was rebuilt. Specifically, the nitroxide spin label was oriented by using the optimized γ and η angles. The resultant, "dynamic" structural model of the alanine-based peptide is shown in Figure 8b.

The average Cu^{2+}−nitroxide distance in the folded state of the alanine-based peptide has been measured to be 25 ± 0.8 Å at physiological temperatures by using the effects of Cu^{2+} on the T_1 value of the nitroxide.[65] As pointed out by these authors, this distance is expected to be shorter than the actual average, since T_1 enhancements depend on r^{-6} rather than r. Indeed, we obtained a mean distance of 27 Å. In comparison, the average

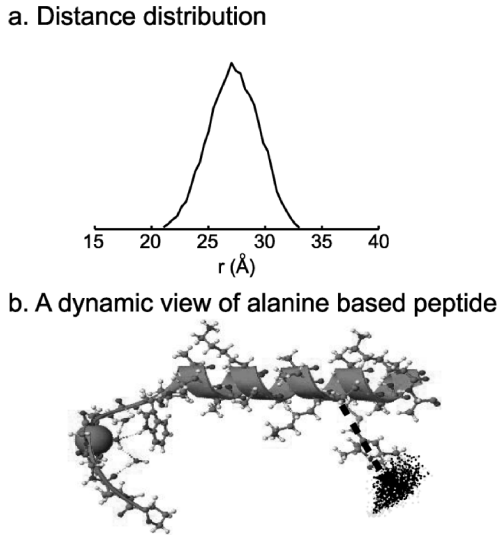

Figure 8. (a) The determined Cu^{2+}−nitroxide distance distribution function using the molecular model. (b) A "dynamic" view of the alanine-based peptide.

distance from the Tikhonov method is smaller than 25 Å (cf. the Supporting Information). The measurement of the distance distribution allows us to make a closer comparison. The value of r_{ESR}, measured by a relaxation based measurement, as shown by Jun et al.,[65] is given by

$$r_{ESR} = \kappa^{1/6} \cdot \left[\left\{ \sum_{r_1}^{r_2} P(r) \left(\frac{\kappa}{r^6} + \frac{1}{T_{1s}^0} \right) \right\} - \frac{1}{T_{1s}^0} \right]^{-1/6} \quad (3)$$

where κ is a constant as defined previously,[65] T_{1s}^0 is the longitudinal relaxation time of the "slow" relaxing spin, the nitroxide, in the absence of Cu^{2+}, $P(r)$ is the distance distribution between Cu^{2+} and nitroxide spins, and r is the real Cu^{2+}−nitroxide distance in each conformation of the peptide.[65] Using the same T_{1s}^0 and T_{1s} values as Jun et al.,[65] we obtained a 25.7 Å "ESR averaged" Cu^{2+}−nitroxide distance using eq 3, consistent with the previous results.[65] In contrast, using the distance distributions obtained from the Tikhonov regularization method (see the Supporting Information), we obtained "ESR averaged" Cu^{2+}−nitroxide distances of 21−23 Å, 2−3 Å shorter than the previous results.[65] This further verifies that, to obtain precise distance distributions between Cu^{2+} and nitroxide spin centers, full data analysis is required.

DEER on the Proline-Based Peptide. The proline-based peptide contains two copper centers separated by seven prolines. Similar to the alanine-based peptide sample, the Cu^{2+} binding environment in the proline-based peptide was also confirmed by using three-pulse electron spin echo envelop modulation (ESEEM) spectroscopy (data not shown).[67] The experimental DEER traces on the proline-based peptide are shown in Figure 9a. The observer pulses were applied at five different magnetic fields scanning from the $g_\perp$ region to the $g_\parallel$ region, as indicated by the arrows in the inset to Figure 9a. The pump pulse was applied at a frequency 92 MHz lower than the observer frequency. The zero time of each data set was precisely determined and illustrated by the dashed line in Figure 9a. Depending on the external magnetic field, the modulation depth for each data set is 0.5−2%, consistent with theoretical calculations.[1] In the raw data, a modulation can be visualized before baseline correction. After baseline correction by using

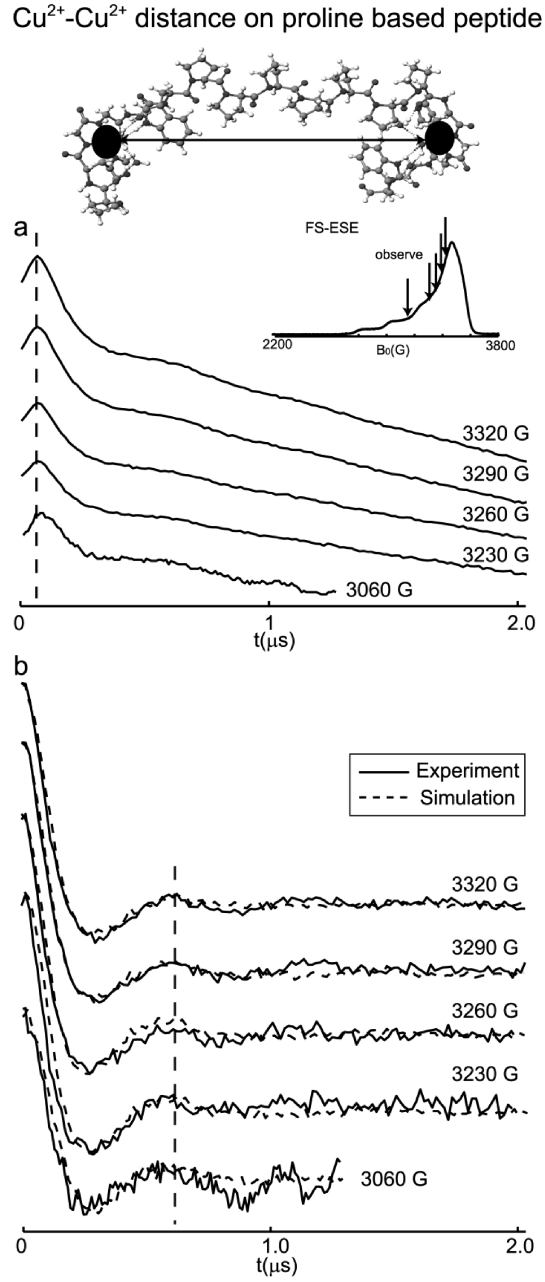

Figure 9. (a) Experimental DEER time domain traces for the proline-based peptide at five magnetic fields between 3060 and 3320 G. The vertical dashed line indicates the zero time of each trace. (Inset) The FS-ESE spectrum of the proline-based peptide with observer frequencies indicated by arrows. The pump pulse was kept 90 MHz lower than the observer frequency in all of the data sets. (b) DEER signal after the removal of the intermolecular decay by division of an exponential decay. At the $g_\perp$ region, the modulation period is ∼600 ns. At the $g_\parallel$ region, the modulation period shifts to ∼540 ns. These baseline corrected DEER data were fit by using the theoretical model developed in this work. Simulations are shown by dashed lines.

an exponential function, the results are shown in Figure 9b. The modulation curve did not change appreciably among the data sets in the $g_\perp$ region. The first period of modulation ends at ∼600 ns for each data set. At the $g_\parallel$ region, the first period of modulation ends at ∼540 ns, which differs distinctively from other data sets (cf. the vertical dashed line).

Before fitting the experimental data, a raw structure of the peptide was constructed by using the CAChe 6.12 package using the following procedures. The seven prolines were built to form a PPII conformation. The structures of the two Cu^{2+}−PHGGGW

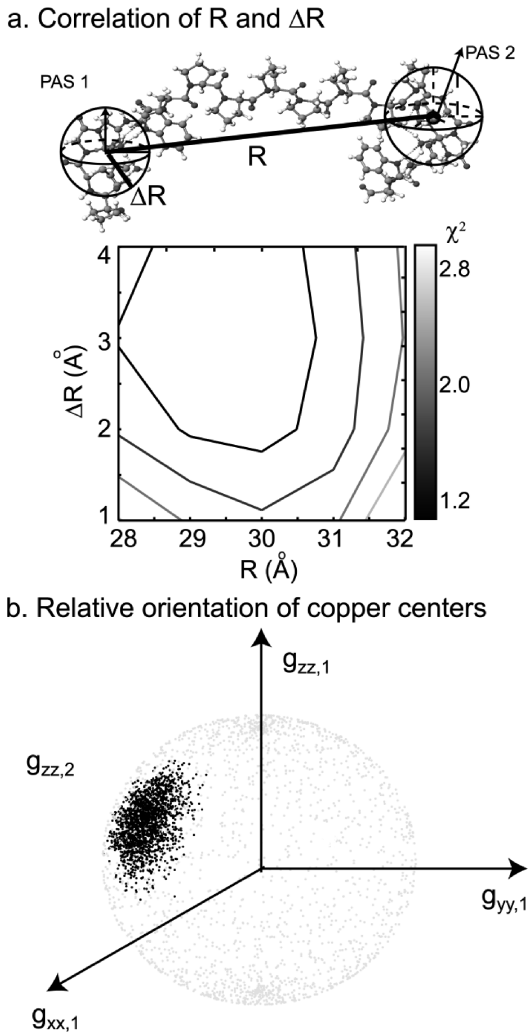

Figure 10. (a) Correlation between R and ΔR, using initial inputs of $\chi = 90°$, $\gamma = 0°$, and $\eta = 60°$. The lowest χ^2 value occurs at $R = 30$ Å, $\Delta R = 3$ Å, $\chi = 60°$, $\gamma = 60°$, and η=0°. (b) Orientations of the second Cu^{2+} g_{zz} axis with respect to the first Cu^{2+} g-tensor shown by black dots.

groups were adapted from the crystal structure obtained by Millhauser and co-workers.[67] The two Cu^{2+}−PHGGGW groups were connected to both ends of the seven-proline segment. The binding angles and dihedral angles between the PHGGGW groups and the seven-proline segment were adapted from Becker et al., where two Cu^{2+} bound PHGGGW groups were attached to a three proline segment.[64] The resultant proline-based peptide is shown in Figure 2b. The Euler angles are measured to be $\chi = 60°$, $\gamma = 30°$, and $\eta = 0°$ in this model. These Euler angles were used as the initial inputs. The standard deviation was assumed to be the same for all three Euler angles, at 20°. The correlation of R and ΔR was calculated and shown in Figure 10a. The best fit occurred at $R = 30$ Å and $\Delta R = 3$ Å. We then fixed R and ΔR at the preoptimized values and optimized the other parameters. The best fit occurred at $(\chi, \gamma, \eta) = (60°, 60°, 0°)$ and $\sigma = 9-12°$. Using these Euler angles and deviations, the R and ΔR correlation was checked again. The best fit still occurred at $R = 30$ Å and $\Delta R = 3$ Å. Using the optimized parameter set, the relative orientations between Cu^{2+} g-tensors can be illustrated by the black dots shown in Figure 10b. The specificity of the optimized Euler angles, $\chi = 60°$, $\gamma = 60°$, and $\eta = 0°$, was further examined by investigating the change of the average χ^2 values upon changing the Euler angles. Details are provided in the Supporting Information. Similar to the fitting

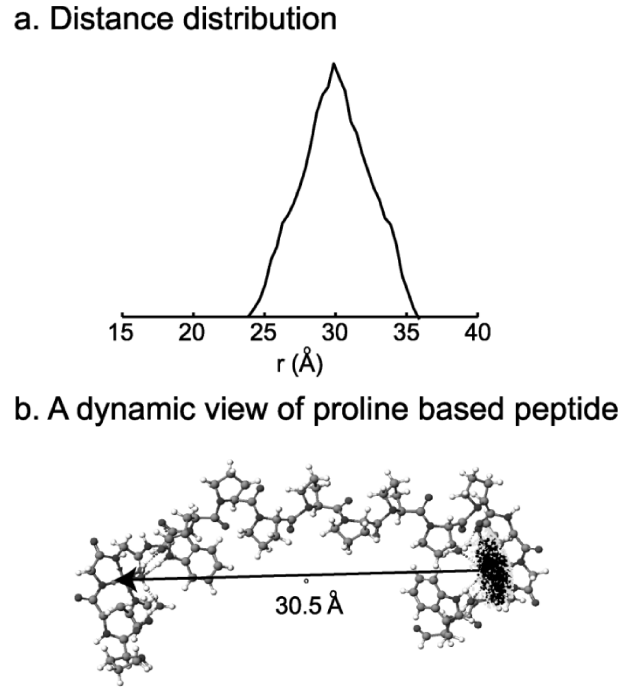

Figure 11. (a) The determined $Cu^{2+}-Cu^{2+}$ distance distribution function using the molecular model. (b) A "dynamic" view of the proline-based peptide obtained based on the relative orientation and flexibility determined from the analysis of the DEER data on the proline-based peptide.

procedure for the alanine-based peptide, up to five other initial inputs were tested for the proline-based peptide. Our simulations showed that the optimized parameter set and distance distribution function were unaffected.

The $Cu^{2+}-Cu^{2+}$ distance distribution was calculated by a statistical histogram plot of the spin−spin distances for 2000 conformations generated using our model and shown by the solid line in Figure 11a. The mean distance and standard deviation was calculated to be 30 and 2.4 Å, respectively. The average $Cu^{2+}-Cu^{2+}$ distance is consistent with the structural model shown in Figure 2b. The standard deviation is in agreement with literature estimates of polyproline peptides.[63] Similar to the alanine-based peptide, the large σ values are reasonable given that a small bending of the proline-based peptide can lead to a large change in the relative orientation between Cu^{2+} centers. The distance distribution function obtained from our molecular model was compared with that from the Tikhonov regularization method (cf. Figure S4 in the Supporting Information). The deviation between these distribution functions indicates that, to obtain precise $Cu^{2+}-Cu^{2+}$ distances, a full data analysis is required. Using the determined Euler angles and standard deviations of these angles, the model of the proline-based peptide was rebuilt. Specifically, the position and the orientation of the second copper center with respect to the first copper center were determined by the optimized variables in the model. The resultant, "dynamic" structural model of the proline-based peptide is shown in Figure 11b.

Role of σ in Reducing Orientational Effects. For both peptides, the flexibilities of the Euler angles reduced the orientational selectivity of the simulated DEER signal compared to the single crystal state. This is reflected by representative calculations of the geometrical factor shown in Figure 12 for the proline-based peptide at two magnetic fields. In Figure 12, at two different magnetic fields, $\sigma = 1°$ leads to extremely

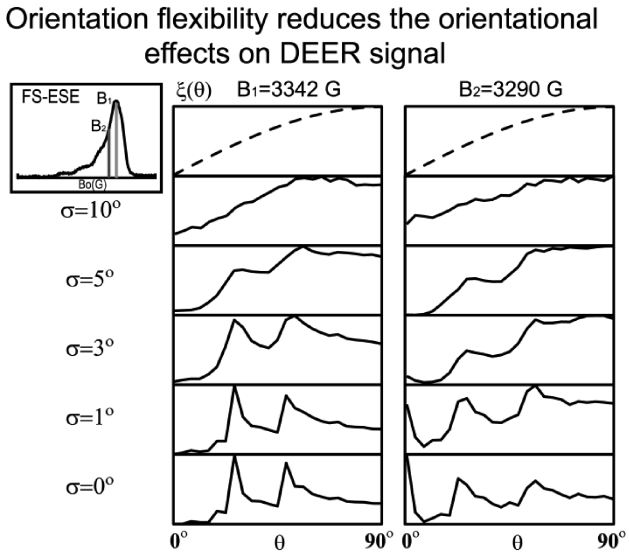

Figure 12. Representative calculations of the geometrical factor for the proline-based peptide at two magnetic fields, 3342 and 3290 G. As σ increases, the θ excitation profiles show that more θ angles are excited, indicating that the orientational selectivity is reduced. (Inset) Field-swept electron spin echo spectrum with the two magnetic fields indicated.

different θ excitation profiles. Strong orientational selectivity of the DEER signal can, therefore, be anticipated in cases of smaller σ.[54] Our simulations also confirmed this consequence. As σ increases, the θ excitation profiles for both magnetic fields become broader, indicating that more θ angles are excited. However, the excitation probabilities for different θ angles are not uniform. Therefore, the case of $\sigma = 10°$ is not sufficient to completely wash out the orientational selectivity, and we still anticipate observing weak orientational effects on the DEER signal, as confirmed by our simulations. As σ increases to higher values, the orientational selectivity further reduces.

Conclusions

We show DEER data on a bis-Cu^{2+}-labeled peptide and a Cu^{2+}−nitroxide labeled peptide. DEER experiments were performed at several external magnetic fields and resonance offsets, to probe the orientational effects on the Cu^{2+}-based DEER signal. Subtle but detectable orientational effects were observed from the DEER spectra of both peptides at the X-band. A general theoretical model was developed to analyze the experimental data sets. A 30 Å mean Cu^{2+}−Cu^{2+} distance and a 27 Å mean Cu^{2+}−nitroxide distance were determined. The relative orientation of spin centers was also determined from the molecular model for both peptides. We show that to obtain precise Cu^{2+}-based distance distributions a full data analysis procedure that incorporates orientational effects is required. Our data analysis procedure is applicable to an unknown, larger sample.

Acknowledgment. This research was supported by NSF (MCB 0842956). We thank Prof. Sarah Larsen and Dr. William Ames for providing the spin density distribution in the Cu^{2+} bound PGHHHW group. We also thank Ming Ji for the spin density distribution calculations using the ORCA package.

Supporting Information Available: Some theoretical aspects of Cu^{2+}-based DEER signal calculation, supplemental fitting to the data on the proline-based peptide, and distance distributions obtained from Tikhonov regularization for the two polypeptides. This material is available free of charge via the Internet at http://pubs.acs.org.

References and Notes

(1) Milov, A.; Ponomerev, A.; Tsvetkov, Y. *Chem. Phys. Lett.* **1984**, *110*, 67.
(2) Larson, R. G.; Singel, D. J. *J. Chem. Phys.* **1993**, *98*, 5134.
(3) Martin, R. E.; Pannier, M.; Diederich, F.; Gramlich, V.; Hubrich, M.; Spiess, H. W. *Angew. Chem., Int. Ed.* **1998**, *37*, 2834.
(4) Pannier, M.; Veit, S.; Godt, A.; Jeschke, G.; Spiess, H. *J. Magn. Reson.* **2000**, *142*, 331.
(5) Elsasser, C.; Brecht, M.; Bittl, R. *J. Am. Chem. Soc.* **2002**, *124*, 12606.
(6) Amsterdam, I. M. C. v.; Ubbink, M.; Canters, G. W.; Huber, M. *Angew. Chem., Int. Ed.* **2003**, *42*, 62.
(7) Bennati, M.; Robblee, J.; Mugnaini, V.; Stubbe, J.; Freed, J.; Borbat, P. *J. Am. Chem. Soc.* **2005**, *127*, 15014.
(8) Kawamori, A.; Ono, T.-A.; Ishii, A.; Nakazawa, S.; Hara, H.; Tomo, T.; Minagawa, J.; Bittl, R.; Dzuba, S. A. *Photosynth. Res.* **2005**, *84*, 187.
(9) Astashkin, A. V.; Seravalli, J.; Mansoorabadi, S. O.; Reed, G. H.; Ragsdale, S. W. *J. Am. Chem. Soc.* **2006**, *128*, 3888.
(10) Banham, J.; Timmel, C.; Abbott, R.; Lea, S.; Jeschke, G. *Angew. Chem., Int. Ed.* **2006**, *45*, 1058.
(11) Fajer, P. G.; Gyimesi, M. a. e.; Málnási-Csizmadia, A.; Bagshaw, C. R.; Sen, K. I.; Song, L. *J. Phys: Condens. Matter* **2007**, *19*, 1.
(12) Denysenkov, V. P.; Biglino, D.; Lubitz, W.; Prisner, T. F.; Bennati, M. *Angew. Chem., Int. Ed.* **2008**, *47*, 1224.
(13) Klein, J. C.; Burr, A. R.; Svensson, B.; Kennedy, D. J.; Allingham, J.; Titus, M. A.; Rayment, I.; Thomas, D. D. *Proc. Natl. Acad. Sci. U.S.A.* **2008**, *105*, 12867.
(14) Swanson, M. A.; Kathirvelu, V.; Majtan, T.; Frerman, F. E.; Eaton, G. R.; Eaton, S. S. *J. Am. Chem. Soc.* **2009**, *131*, 15978.
(15) Kear, J. L.; Blackburn, M. E.; Veloro, A. M.; Dunn, B. M.; Fanucci, G. E. *J. Am. Chem. Soc.* **2009**, *131*, 14650.
(16) Ghimire, H.; McCarrick, R. M.; Budil, D. E.; Lorigan, G. A. *Biochemistry* **2009**, *48*, 5782.
(17) Galiano, L.; Blackburn, M. E.; Veloro, A. M.; Bonora, M.; Fanucci, G. E. *J. Phys. Chem. B* **2009**, *113*, 1673.
(18) Galiano, L.; Ding, F.; Veloro, A. M.; Blackburn, M. E.; Simmerling, C.; Fanucci, G. E. *J. Am. Chem. Soc.* **2009**, *131*, 430.
(19) Schiemann, O.; Piton, N.; Mu, Y.; Stock, G.; Engels, J. W.; Prisner, T. F. *J. Am. Chem. Soc.* **2004**, *126*, 5722.
(20) Ward, R.; Keeble, D. J.; El-Mkami, H.; Norman, D. G. *ChemBioChem* **2007**, *8*, 1957.
(21) Schiemann, O.; Piton, N.; Plackmeyer, J.; Bode, B. E.; Prisner, T. F.; Engels, J. W. *Nat. Protoc.* **2007**, *2*, 904.
(22) Qin, P. Z.; Haworth, I. S.; Cai, Q.; Kusnetzow, A. K.; Grant, G. P. G.; Price, E. A.; Sowa, G. Z.; Popova, A.; Herreros, B.; He, H. *Nat. Protoc.* **2007**, *2*, 2354.
(23) Sicoli, G.; Mathis, G.; Delalande, O.; Boulard, Y.; Gasparutto, D.; Gambarelli, S. *Angew. Chem., Int. Ed.* **2008**, *47*, 735.
(24) Kuznetsov, N. A.; Milov, A. D.; Koval, V. V.; Samoilova, R. I.; Grishin, Y. A.; Knorre, D. G.; Tsvetkov, Y. D.; Fedorova, O. S.; Dzuba, S. A. *Phys. Chem. Chem. Phys.* **2009**, *11*, 6826.
(25) Milov, A. D.; Maryasov, A. G.; Tsvetkov, Y. D.; Raap, J. *Chem. Phys. Lett.* **1999**, *303*, 135.
(26) Pannier, M.; Schöps, M.; Schädler, V.; Wiesner, U.; Jeschke, G.; Spiess, H. W. *Macromolecules* **2001**, *34*, 5555.
(27) Pornsuwan, S.; Bird, G.; Schafmeister, C.; Saxena, S. *J. Am. Chem. Soc.* **2006**, *128*, 3876.
(28) Bode, B. E.; Margraf, D.; Plackmeyer, J.; Dürner, G.; Prisner, T. F.; Schiemann, O. *J. Am. Chem. Soc.* **2007**, *129*, 6736.
(29) Margraf, D.; Bode, B. E.; Marko, A.; Schiemann, O.; Prisner, T. F. *Mol. Phys.* **2008**, *105*, 2153.
(30) Lovett, J. E.; Hoffmann, M.; Cnossen, A.; Shutter, A. T. J.; Hogben, H. J.; Warren, J. E.; Pascu, S. I.; Kay, C. W. M.; Timmel, C. R.; Anderson, H. L. *J. Am. Chem. Soc.* **2009**, *131*, 13852.
(31) Gordon-Grossman, M.; Gofman, Y.; Zimmermann, H.; Frydman, V.; Shai, Y.; Ben-Tal, N.; Goldfarb, D. *J. Phys. Chem. B* **2009**, *113*, 12687.
(32) Gulla, S. V.; Sharma, G.; Borbat, P.; Freed, J. H.; Ghimire, H.; Benedikt, M. R.; Holt, N. L.; Lorigan, G. A.; Rege, K.; Mavroidis, C.; Budil, D. E. *J. Am. Chem. Soc.* **2009**, *131*, 5374.
(33) Park, S.-Y.; Borbat, P. P.; Gonzalez-Bonet, G.; Bhatnagar, J.; Pollard, A. M.; Freed, J. H.; Bilwes, A. M.; Crane, B. R. *Nat. Struct. Biol.* **2006**, *13*, 400.
(34) Borovykh, I. V.; Ceola, S.; Gajula, P.; Gast, P.; Steinhoff, H.-J. r.; Huber, M. *J. Magn. Reson.* **2006**, *180*, 178.
(35) Hilger, D.; Polyhach, Y.; Padan, E.; Jung, H.; Jeschke, G. *Biophys. J.* **2007**, *93*, 3675.
(36) Milov, A. D.; Tsvetkov, Y. D.; Gorbunov, E. Y.; Mustaeva, L. G.; Ovchinnikova, T. V.; Handgraaf, J.-W.; Raap, J. *Chem. Biodiversity* **2007**, *4*, 1243.

(37) Vamvouka, M.; Cieslak, J.; Eps, N. V.; Hubbell, W.; Gross, A. *Protein Sci.* **2008**, *17*, 506.
(38) Upadhyay, A. K.; Borbat, P. P.; Wang, J.; Freed, J. H.; Edmondson, D. E. *Biochemistry* **2008**, *47*, 1554.
(39) Kim, M.; Xu, Q.; Murray, D.; Cafiso, D. S. *Biochemistry* **2008**, *47*, 670.
(40) Altenbach, C.; Kusnetzow, A. K.; Ernst, O. P.; Hofmann, K. P.; Hubbell, W. L. *Proc. Natl. Acad. Sci. U.S.A.* **2008**, *105*, 7439.
(41) Zou, P.; Bortolus, M.; Mchaourab, H. S. *J. Mol. Biol.* **2009**, *393*, 586.
(42) Meyer, S.; Bo¨hme, S.; Krüger, A.; Steinhoff, H.-J.; Klare, J. P.; Wittinghofer, A. *PLoS Biol.* **2009**, *7*, 1.
(43) Herrick, D. Z.; Kuo, W.; Huang, H.; Schwieters, C. D.; Ellena, J. F.; Cafiso, D. S. *J. Mol. Biol.* **2009**, *390*, 913.
(44) Hagelueken, G.; Ingledew, W. J.; Huang, H.; Petrovic-Stojanovska, B.; Whitfield, C.; ElMkami, H.; Schiemann, O.; Naismith, J. H. *Angew. Chem., Int. Ed.* **2009**, *48*, 2904.
(45) Dockter, C.; Volkov, A.; Bauer, C.; Polyhach, Y.; Joly-Lopez, Z.; Jeschke, G.; Paulsen, H. *Proc. Natl. Acad. Sci. U.S.A.* **2009**, *106*, 18485.
(46) Sen, K. I.; Logan, T. M.; Fajer, P. G. *Biochemistry* **2007**, *46*, 11639.
(47) Stone, K. M.; Townsend, J. E.; Sarver, J.; Sapienza, P. J.; Saxena, S.; Jen-Jacobson, L. *Angew. Chem., Int. Ed.* **2008**, *47*, 1.
(48) Altenbach, C.; Flitsch, S. L.; Khorana, H. G.; Hubbell, W. L. *Biochemistry* **1989**, *28*, 7806.
(49) Hubbell, W. L.; Cafiso, D. S.; Altenbach, C. *Nat. Struct. Biol.* **2000**, *7*, 735.
(50) Hubbell, W.; Gross, A.; Langen, R.; Lietzow, M. *Curr. Opin. Struct. Biol.* **1998**, *8*, 649.
(51) Chiang, Y.-W.; Borbat, P.; Freed, J. H. *J. Magn. Reson.* **2005**, *172*, 279.
(52) Jeschke, G.; Chechik, V.; Ionita, P.; Godt, A.; Zimmermann, H.; Banham, J.; Timmel, C. R.; Hilger, D.; Jung, H. *Appl. Magn. Reson.* **2006**, *30*, 473.
(53) Narr, E.; Godt, A.; Jeschke, G. *Angew. Chem., Intl. Ed.* **2002**, *41*, 3907.
(54) Yang, Z.; Becker, J.; Saxena, S. *J. Magn. Reson.* **2007**, *188*, 337.
(55) Kay, C. W. M.; Mkami, H. E.; Cammack, R.; Evans, R. W. *J. Am. Chem. Soc.* **2007**, *129*, 4868.
(56) Bode, B. E.; Plackmeyer, J.; Prisner, T. F.; Schiemann, O. *J. Phys. Chem. A* **2008**, *112*, 5064.
(57) Lovett, J. E.; Bowen, A. M.; Timmel, C. R.; Jones, M. W.; Dilworth, J. R.; Caprotti, D.; Bell, S. G.; Wong, L. L.; Harmer, J. *Phys. Chem. Chem. Phys.* **2009**, *11*, 6840.
(58) Milikisyants, S.; Scarpelli, F.; Finiguerra, M. G.; Ubbink, M.; Huber, M. *J. Magn. Reson.* **2009**, *201*, 48.
(59) Endeward, B.; Butterwick, J. A.; MacKinnon, R.; Prisner, T. F. *J. Am. Chem. Soc.* **2009**, *131*, 15246.
(60) Denysenkov, V. P.; Prisner, T. F.; Stubbe, J.; Bennati, M. *Proc. Natl. Acad. Sci. U.S.A.* **2006**, *103*, 13386.
(61) Polyhach, Y.; Godt, A.; Bauer, C.; Jeschke, G. *J. Magn. Reson.* **2007**, *185*, 118.
(62) Gnanakaran, S.; Hochstrasser, R. M.; Gacia, A. E. *Proc. Natl. Acad. Sci. U.S.A.* **2004**, *101*, 9229.
(63) Schuler, B.; Lipman, E. A.; Steinbach, P. J.; Kumke, M.; Eaton, W. A. *Proc. Natl. Acad. Sci. U.S.A.* **2005**, *102*, 2754.
(64) Becker, J.; Saxena, S. *Chem. Phys. Lett.* **2005**, *414*, 248.
(65) Jun, S.; Becker, J.; Yonkunas, M.; Coalson, R.; Saxena, S. *Biochemistry* **2006**, *45*, 11666.
(66) Maryasov, A. G.; Tsvetkov, Y. D.; Raap, J. *Appl. Magn. Reson.* **1998**, *14*, 101.
(67) Aronoff-Spencer, E.; Burns, C. S.; Avdievich, N. I.; Gerfen, G. J.; Peisach, J.; Antholine, W. E.; Ball, H. L.; Cohen, F. E.; Prusiner, S. B.; Millhauser, G. L. *Biochemistry* **2000**, *39*, 13760.
(68) Ames, W. M.; Larsen, S. C. *J. Biol. Inorg. Chem.* **2009**, *14*, 14547.
(69) Burns, C.; Aronoff-Spencer, E.; Dunham, C.; Lario, P.; Avdievich, N.; Antholine, W.; Olmstead, M.; Vrielink, A.; Gerfen, G.; Peisach, J.; Scott, W.; Millhauser, G. *Biochemistry* **2002**, *41*, 3991.
(70) Millhauser, G. L. *Acc. Chem. Res.* **2004**, *37*, 79.

JP911637S